UNIVERSITY of CALIFORNIA
UNIVERSITY OF CALIFORNIA, SANTA CRUZ

QUANTIFYING STELLAR SUBSTRUCTURE IN THE VIA LACTEA N-BODY COSMOLOGICAL SIMULATION OF THE MILKY WAY DARK HALO

A thesis submitted in partial satisfaction of the
requirements for the degree of

BACHELOR OF SCIENCE

in

ASTROPHYSICS

by

Michael A. Obranovich

10 June 2009

The thesis of Michael A. Obranovich is approved by:

Professor Piero Madau
Technical Advisor

Professor David P. Belanger
Thesis Advisor

Professor David P. Belanger
Chair, Department of Physics

Abstract

Quantifying Stellar Substructure in the Via Lactea N-body Cosmological Simulation of the Milky Way Dark Halo

by

Michael A. Obranovich

We begin by implementing a star formation prescription described by Bullock et al. [4] to model the Stellar Halo of the Milky Way using the Via Lactea I [6] and II [7] simulations. By building the Stellar Halo from the accretion of subunits (subhalos) we can predict the amount of substructure in the Milky Way for comparison with observations. We quantify the degree of "clumpiness" by finding variations in surface brightness within pencil beams of various angular sizes. We find that the stellar halo exhibits the largest amount of clumpiness on small scales of beam sizes ($1-2^\circ$ and $2-4^\circ$) and is rather smooth on larger scales ($4-8^\circ$ and $6-14^\circ$).

Contents

List of Figures

I'd like to dedicate this thesis to my family, whose continual support has helped greatly in this endeavor and will continue to do so as I go on in my studies of Physics.

Acknowledgements

I'd like to thank Professor Piero Madau and Dr. Jürg Diemand for having patience with me and allowing me to work on such an important research project.

1 Introduction

The model of our universe widely accepted today is rather young considering the time-line of modern science beginning with Galileo and Newton. The structure of the universe was only physically explained by Einstein's theory of Gravity, General Relativity (GR). General Relativity describes the geodesic of space-time in terms of a distribution of energy density. Where energy density is negligible, or zero, then space-time is flat and the geodesic is given by the usual one used in special relativity,

$$ds^2 = -c^2dt^2 + dr^2 + r^2d\Omega^2[5]. \tag{1.1}$$

Where $d\Omega^2 = d\theta^2 + sin^2(\theta)d\phi^2$. This metric is altered in GR to take into account curved space-time as

$$ds^2 = g_{\mu\nu}dx^\mu dx^\nu.[5] \tag{1.2}$$

Where $g_{\mu\nu}$ is the metric tensor. If $g_{\mu\nu} = \begin{pmatrix} -c^2 & 0 & 0 & 0 \\ 0 & 1 & 0 & 0 \\ 0 & 0 & 1 & 0 \\ 0 & 0 & 0 & 1 \end{pmatrix}$ then Eq.(1.1) is recovered. There are many different geometries that the metric tensor can describe but we will only be interested in one, the Robertson-Walker metric, which will be discussed in more detail later.

The metric tensor plays an important part in the Einstein equation,

$$R_{ik} - \frac{1}{2}g_{ik}R - \Lambda g_{ik} = \frac{8\pi G}{c^4}T_{ik}[5]. \tag{1.3}$$

Here, in addition to the metric tensor and physical constants, R_{ik} is known as the Ricci tensor, R the Ricci scalar, Λ the Cosmological constant, and finally T_{ik} is the Stress-Energy tensor. Equation (1.3) contains all the necessary information required to describe what space-time looks like and thus

how matter will behave in such a structure. If we can make assumptions about the universe such that we can solve Eq. (1.3) then we will be able to determine the evolution of the universe and its contents as well.

1.1 Cosmology

The universe on very large scales appears to be *homogeneous* and *isotropic*. Postulated by the *Cosmological Principle*, *Isotropy* means that the universe looks the same in any direction as though Earth did not occupy a special place in the universe and *homogeneity* means that the universe is identical everywhere. *Cosmological Principle* requires the energy distribution of the universe to be spread perfectly evenly on average, and in this way it will be much easier to describe. [5]

1.1.1 The Robertson-Walker Metric

An isotropic and homogeneous universe can be described by the Robertson-Walker Metric(RW);

$$ds^2 = -c^2dt^2 + a^2(t)\left[\frac{dr^2}{1-\kappa r^2/R_0^2} + r^2 d\Omega^2\right][11]. \tag{1.4}$$

Equation (1.4) is the RW metric, which is very similar to the flat space-time metric (Eq. (1.1)) except that now there is the parameter $a(t)$ known as the *expansion factor*. κ is the curvature constant and can be either 0,+1 or -1 corresponding to a flat, positive, or negative curvature of radius R_0 [11]. The dimensionless expansion factor scales only with time, and its dependence on time is derived by solving the Friedmann Equation.

We can see the effect of expansion already in that a particle could occupy some coordinate in space, $\vec{x}$, for all time but when one considers a change of coordinates, $\vec{X} = a(t)\vec{x}$, then the particle could occupy a different area of space over time depending on how $a(t)$ varied. The coordinate $\vec{x}$ is known as a *comoving* coordinate and $\vec{X}$ a *proper* coordinate. The distances to objects therefore

obey the equation

$$d(t) = a(t)d_{coord}, \tag{1.5}$$

where $d_{coord} = (\Delta x^2 + \Delta y^2 + \Delta z^2)^{1/2}$ is fixed in time but the physical distance $d(t)$ can change by Eq. (1.5) [9].

The expansion factor allows for a relation to the redshift, z. By definition $z = \frac{\lambda_o - \lambda_e}{\lambda_e}$, where λ_e is the wavelength emitted and λ_o is the observed wavelength. Most shifts in wavelength occur due to relative motions between the observer and emitter. But there is a redshift due to the expansion of space-time where the space between crests of a traveling wave are actually expanded resulting in a redshift. If we consider the null geodesic ($ds^2 = 0$), we can write the comoving distance r as,

$$c\int_{t_e}^{t_0} \frac{dt}{a(t)} = r, \tag{1.6}$$

with t_0 being the present time and t_e the time of emission. This can be readily solved to obtain

$$\frac{a(t_e)}{a(t_0)} = \frac{1}{1+z}, \tag{1.7}$$

the expansion factor-redshift relation [11]. It is convention to set $a(t_0) = 1$, with the Big Bang occurring at $a(t_{bigbang}) = 0$ and therefore $z = \infty$. When we look farther into space (and time as well) we observe objects as being more and more redshifted, and when the velocity redshift equation is taken into account ($v \approx cz$ for small z) it can be concluded that the universe was expanding at a faster rate in the past.

1.1.2 Friedmann Equation

The *Friedmann Equation* comes about from solving Einstein's Equation with g_{ik} is set equal to the RW metric and the stress-energy tensor of a perfect fluid is used for T_{ik}. This equation allows for a solution of the time dependence of the expansion factor, $a(t)$,

$$H^2(t) = H_0^2\left[\frac{\Omega_{0,r}}{a^4(t)} + \frac{\Omega_{0,m}}{a^3(t)} + \frac{\Omega_{0,k}}{a^2(t)} + \Omega_{0,\Lambda}\right], \tag{1.8}$$

$H(t)$ is the *Hubble Parameter* and is equal to $\dot{a}(t)/a(t)$ and H_0 is the Hubble parameter today. The density parameter is defined to be $\Omega_{0,i} = \frac{\rho_{0,i}}{\rho_{0,c}}$, where $\rho_{0,i}$ is the density today of some form of energy, i (m, r, k, Λ), and $\rho_{0,c}$ is the *critical density* today. The present critical density is equal to $\frac{3c^2}{8\pi G}H_0^2 \approx 8.3 \times 10^{-10} Jm^{-3}$[11]. $\Omega_{0,r}$, $\Omega_{0,m}$, $\Omega_{0,k}$, $\Omega_{0,\Lambda}$ correspond to the density parameters of radiation, matter, curvature, and the cosmological constant respectively. If we can measure the different density parameters than we can have a complete picture on how the universe evolves over time, both in the past and in the future.

If $\kappa = 0$ then the density parameters will always add up so

$$\Omega_{0,m} + \Omega_{0,r} + \Omega_{0,\Lambda} = 1. \tag{1.9}$$

So far κ appears to be zero from measured values of the density parameters. The *Wilkinson Microwave Anisotropy Probe* (WMAP) is a project by NASA to determine the contents of the Universe. Data taken from the WMAP survey have provided us with values of $\Omega_{0,dm} = 0.23$, $\Omega_{0,bary} = 0.046$, *and* $\Omega_{0,\Lambda} = 0.72$[3] with $\Omega_{0,r}$ *and* $\Omega_{0,k}$ having negligible values. $\Omega_{0,dm}$ is the Dark Matter component and $\Omega_{0,bary}$ is the baryonic component which add such that,

$$\Omega_{0,dm} + \Omega_{0,bary} = \Omega_{0,m}. \tag{1.10}$$

Λ, (*dark energy*), is dominate today and will be so in the future as well.

1.2 Structure Formation in the Universe

The *Cosmological Principle* states that the universe is homogeneous on large scale distances of $\gtrsim 100 Mpc$. The Cosmic Microwave Background (CMB) (fig. 1.1) shows that the Universe was very homogeneous in the past, so there must be something at work to bring matter in to form the structures of the universe.

The answer lies in *Gravitational Instability*, wherein if a small density fluctuation forms, that fluctuation grows due to gravitational collapse. As the mass of the object increases, its gravity

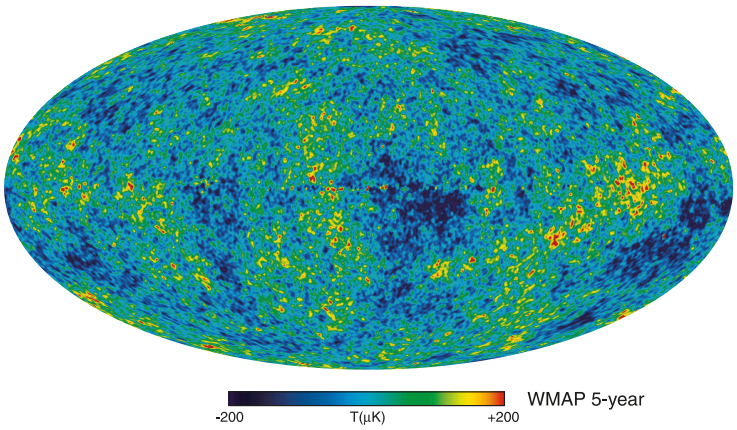

Figure 1.1: The Cosmic Microwave Background radiation from early universe ($z \sim 1100$) taken by the WMAP 5-year survey. The temperature fluctuations are only on the order of $\sim 10^{-5}K$ [10] and imply a very uniform early universe.

increases by $M(< r)$, thus accumulating more and more mass forming a deeper potential well until after enough time, astrophysical structures like stars and galaxies will form. To see how these fluctuations evolve in a pressure-less system (matter only), we can refer to the acceleration equation with zero pressure;

$$\frac{\ddot{a}(t)}{a(t)} = -\frac{4\pi G}{3}\bar{\rho}(t), \tag{1.11}$$

and we will let $\rho(t) = \bar{\rho}(t)[1 + \delta(t)]$. $\delta(t)$ is the density fluctuation $\ll 1$. Using these equations along with the Friedmann Equation we can obtain the following equation,

$$\ddot{\delta}(t) + 2H(t)\dot{\delta}(t) = 4\pi G\bar{\rho}(t)\delta(t). \tag{1.12}$$

If we let H go to zero, then the universe is static, and you can solve the differential equation to get an exponential collapse. The term $2H(t)\dot{\delta}(t)$ is sometimes called the "Hubble Friction" term, of which the expansion of the universe acts against the growth of a density fluctuation and slows down the formation of structures [11].

Perturbations could have began to grow when the Universe had cooled enough at $z \approx 1100$ and would have grown in size by that same factor today. As we will see the perturbations began to grow much sooner ($z \approx 3570$) due to weakly interacting matter which gave early structures a head start in forming before the Universe was cool enough for stars to begin forming.[11]

1.3 Dark Matter

The first evidence for *Dark Matter* (DM) was discovered by Fritz Zwicky in 1933. He used the velocity dispersion of seven different galaxies in the Coma Cluster to estimate a mass to light ratio, Υ, using the *Virial Theorem* [2]. The Virial Theorem for a $1/r$ potential in a stable system takes the form,

$$0 = W + 2K[11]. \tag{1.13}$$

For Newtonian Gravity, $W = \frac{-GM(<r)}{r}$ and $K = \frac{1}{2}mv^2$ with $M(<r)$ being the total mass enclosed by some radius. We can solve for the mass in terms of the rotational velocity (tangential velocity also known as the circular velocity) of an object and its radius from the center of the galaxy. We expect to find the rotational velocity,

$$v_c = \sqrt{\frac{GM(<r)}{r}} \propto \frac{1}{\sqrt{r}}, \tag{1.14}$$

at large enough r. The mass enclosed depends on the density of the galactic disk which falls off exponentially like $\approx \exp\left(-\frac{R}{R_s}\right)$, where $R_s \approx 3.5kpc$. A few multiples of R_s away gives us a reasonably negligible density and thus a constant mass enclosed, so we can assume the velocities do fall off like Eq. (1.14) [11]. In the 1970's it was found that the observed circular velocities didn't fall off but remained nearly constant out to the edge of the galaxies (fig. 1.2). This peculiarity has been reconciled through the idea of DM, matter that interacts with normal *baryonic* matter only through gravity. Since DM does not interact with baryons, no photons are created or reflected and so it remains dark.

Typical values of these "constant" (there is noise but they remain on average constant) rotational velocities are just above $200kms^{-1}$, with our Sun's $v_c \sim 220kms^{-1}$ at a radius $r = 8.5kpc$ from the galactic center (GC). If we consider now a constant velocity instead of a mass, we can rewrite Eq. (1.14) to

$$M(r) = \frac{v^2 r}{G} = 9.6 \times 10^{10} M_\odot \left(\frac{v}{220kms^{-1}}\right)^2 \left(\frac{r}{8.5kpc}\right).[11] \tag{1.15}$$

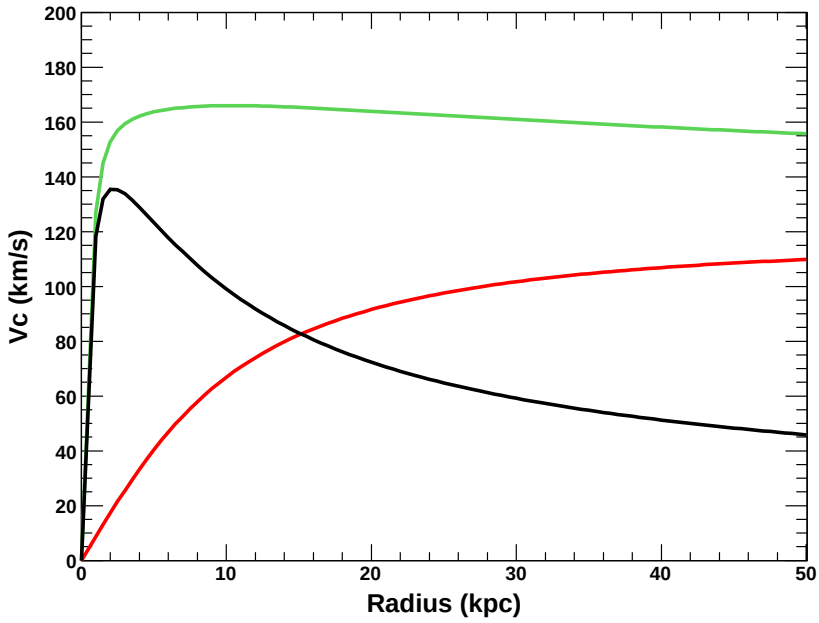

Figure 1.2: Three rotation curves for different density profiles. The Black curve uses the following form $I(r) = \exp(-r/3.5kpc)$ where $I(r)$ is the surface brightness profile of typical galaxies representing the stellar mass. The Red curve is given by the dark halo density $\rho_d(r) = \frac{\rho_0}{1+(r/8.5kpc)^\gamma}$ where $\gamma = 2.1$. [2] Lastly the Green curve is the sum of the two velocity curves and resembles observations.

If we scale the quantities to the properties of the sun, we can obtain a reference to just how much DM there is in our galaxy by looking at the Milky Way's Mass to Light Ratio, Υ. The luminosity of the galaxy is estimated to be $L_{gal} = 2.3 \times 10^{10} L_\odot$, dividing Eq. (1.15) by this value we get

$$\Upsilon \approx 50 \frac{M_\odot}{L_\odot} \left(\frac{R_{halo}}{100kpc} \right). [11] \tag{1.16}$$

R_{halo} is not exactly known, but from Globular Cluster observations it appears to go out to $\sim 75kpc$, giving us $\Upsilon \approx 38 M_\odot / L_\odot$. This implies the dark halo is an order of magnitude more massive than the stellar halo.

1.3.1 The Nature of Dark Matter

So far gravity has been the only lens with which we can observe DM. Just what exactly DM *is* has been one of the questions of the century in Cosmology. Some candidates for DM include

baryonic matter that we just can't see, either primordial black holes, brown dwarfs or interstellar gas. But none of those things are enough to account for so much missing mass. Many have considered the neutrino since it is very weakly interacting, with a cross section $\sim 10^{-49}m^2$ [12]. Although there is a high density of neutrinos ($n_\nu \sim 10^8 m^{-3}$) [11], they have very little mass ($\sim 4eV/c^2$). If we use the neutrino mass observed from solar neutrinos, then they would only contribute to the universe $\Omega_\nu \sim 10^{-3}$. Not nearly enough to account for all the dark matter [11].

There have been many exotic candidates such as *axions* and others which stem from models of particle physics beyond the *Standard Model*. Suppersymmetry offers a slew of potential DM particles including photinos, gravitinos, axinos, sneutrinos and gluinos. These particles are thought to be weakly interacting but are very massive with $mc^2 > 10GeV$. These candidates of DM are known as *Weakly Interacting Massive Particles* or WIMPs. There have been efforts to detect such particles but none have been found as of yet [11].

1.3.2 Cold Dark Matter (CDM) and Substructure

Since the DM is weakly interacting, then as far as we know it was not affected by high radiation and gas pressures in the hot early universe. So as baryonic matter needed time to cool ($z \sim 1100$) before density perturbations could form and grow, the DM had a head start ($z \sim 3570$). DM also makes up a considerable amount more of the total matter in the universe ($\sim 5\Omega_{bary}$), therefore it can be argued that DM is dominant in the formation of structure in the Universe.

The state of the DM in the early universe ($z > 1100$) is key in determining how perturbations can grow. If the DM is *hot* (DM particles are relativistic from the time they decouple from the other components of the universe, until the mass enclosed in a Hubble Volume (c/H) is larger than compared with the mass of galaxies) then the particles moving close to the speed of light wipe out any density fluctuations (known as *free streaming*) on a scale of $\sim ct_{age}$ [11], where t_{age} is the age of the universe at that time. At $z \sim 3570$ the universe was $\approx 65kyr$ old giving a a size scale of

$$\lambda = ct_{age} \approx 20kpc. \tag{1.17}$$

If we consider a comoving size scale $L_{co} = \frac{\lambda}{a(t_{age})}$ then we can get a mass scale estimate independent of the expanding universe.

$$L_{co} = \lambda(1+z) \approx 70Mpc, \tag{1.18a}$$

$$M = \frac{4\pi}{3} L_{co}^3 \Omega_{m,0} \rho_{c,0} = \frac{4\pi}{3}(70Mpc)^3(0.27)(1.35 \times 10^{11} M_\odot Mpc^{-3}) \approx 5 \times 10^{16} M_\odot \tag{1.18b}$$

For Ω_m equal to 0.27. Therefore all density fluctuations smaller than $\sim 10^{16} M_\odot$ (the size of superclusters) will never form [11]. As a result, we should see structures larger than this forming first as those will be the only fluctuations able to form and grow. Observations tell us, however, that structures the size of galaxies ($M \sim 10^{12} M_\odot$) form first and superclusters are now beginning to collapse. This is known as *bottom-up* formation where smaller structures (ie. dwarf galaxies) form first and then larger structures come about later. Since this *is* what we observe, CDM is the leading theory on large-scale structure formation of the universe. On the galactic scale ($M \sim 10^{12} M_\odot$) smaller substructures form and accrete onto large structures until a galactic DM halo is formed. These "subhalos" vary in size, are believed to be the seeds of star formation, and form "stream" like structures when they accrete. Streams are key structures within galaxies and are a growing area of research for both observers and theorists.

1.4 N-body Simulations

Structure formation theory is tested through the means of N-body computer simulations. Higher resolutions are achieved by increasing the amount of particles, N, and decreasing the time steps, ΔT. Advances in computing technology and algorithms have allowed for the study of substructures with masses $M \sim 10^6 M_\odot$[7] within the Milky Way. The Parallel K-D tree Gravity code (PKDGRAV) is a commonly used algorithm for calculating forces on each particle. By using multipole expansions and cells (volumes containing a mass distribution, fig. 1.3) instead of individual particles, efficiency is increased while maintaining accuracy and allowing for increased N. The many cells can be distributed to different parallel processors (thousands in the case of a super computer)

so that efficiency is increased once again.[14]

A force softening parameter ϵ is also used when computing the forces, where the force on a particle $\vec{F}_i$ from all of the other particles is

$$\vec{F}_i = \sum_{j=1}^{N} \frac{Gm^2(\vec{x}_j - \vec{x}_i)}{(\epsilon^2 + |\vec{x}_i - \vec{x}_j|^2)^{3/2}}. \tag{1.19}$$

In this way large forces are avoided when particles with a singular dimension come in close proximity. The large accelerations decrease the time step ($\Delta T \propto (F/\ddot{F})^{1/2}$) and thus increase the computing time.

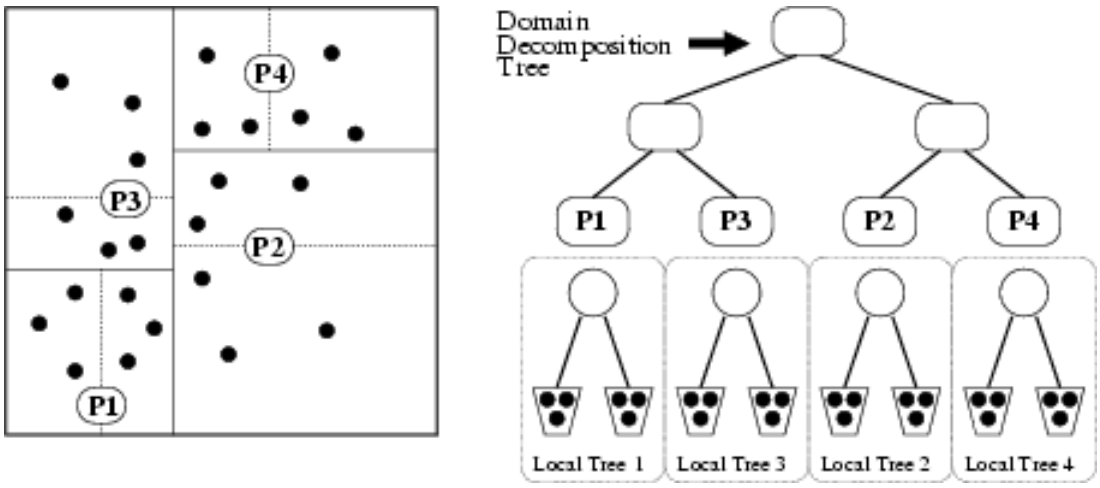

Figure 1.3: A Two-dimensional k-D Tree distributed over four processors. A hierarchy of *buckets* are formed such that there are no more than eight particles in a bucket. The particles within a bucket are set to interact by a fourth-order multipole expansion with all other buckets unless a bucket happens to be within the opening radius (a radius of a bucket determined by the maximum distance from a particle in the bucket to the center of mass). If the opening radius of a bucket intersects the bucket in question, then all of the particles in both buckets are called to interact via a particle-particle interaction (Eq. (1.19)). The task of Calculating the buckets is divided among the number of processors available increasing efficiency [13]. By calculating forces between buckets, of which there are fewer than the total amount of particles, force calculations are far more computationally efficient while maintaining accuracy.

2 Via Lactea

Via Lactea, (Latin for "Milky Way"), is an N-body Cosmological simulation of the Milky Way dark matter halo. There are two such simulations, VL [6] and VL-2 [7], each using a total halo mass $\sim 2 \times 10^{12} M_{\odot}$. VL uses a force softening of 90 pc (40 pc for VL-2) and a time step of $0.2\sqrt{\epsilon/|\vec{a}|}$ while VL-2 uses a time step of $0.06\sqrt{1/G\rho_{enc}}$. The individual time step for each particle is determined by dividing 13.7 Gyr/400 by two until a value less than ΔT is reached. $|\vec{a}|$ is the norm of the acceleration and ρ_{enc} is the enclosed density within the dominant structure at that time [7].

One of the main differences with VL-2 is that nearly five times as many particles are used, bringing N up to 1.1×10^9 resulting in a mass of $4,100 M_{\odot}$ for each particle (opposed to $21,000 M_{\odot}$ for VL) [7]. The local DM densities from each simulation are presented in figure 2.1. One key difference in VL-2 is the increased amount of substructure in the form of DM subhalos. There is as much as 1.97 times as many resolved subhalos in VL-2 as VL with a $V_{max} > 0.25 kms^{-1}$ [7]. V_{max} is the peak circular velocity (the maximum of Eq. (1.14)), $V_{max} = \sqrt{GM(< r_{vmax})/r_{vmax}}$, where r_{vmax} is the radius where the peak circular velocity is reached. As these subhalos pass by the GC they become disrupted and lose matter due to tidal forces. One subhalo can make several passes, accreting material each time onto the host halo, leaving a smaller and smaller remnant. Figure 2.2 displays such an occurrence with an isolated subhalo from VL. Hundreds of the larger subhalos (with $V_{max} > 15 kms^{-1}$) accrete onto the host halo over the course of the simulation resulting in a chaotic assortment of structures. The Dark Halo built upon the larger subhalo accretions only is shown in figure 2.3.

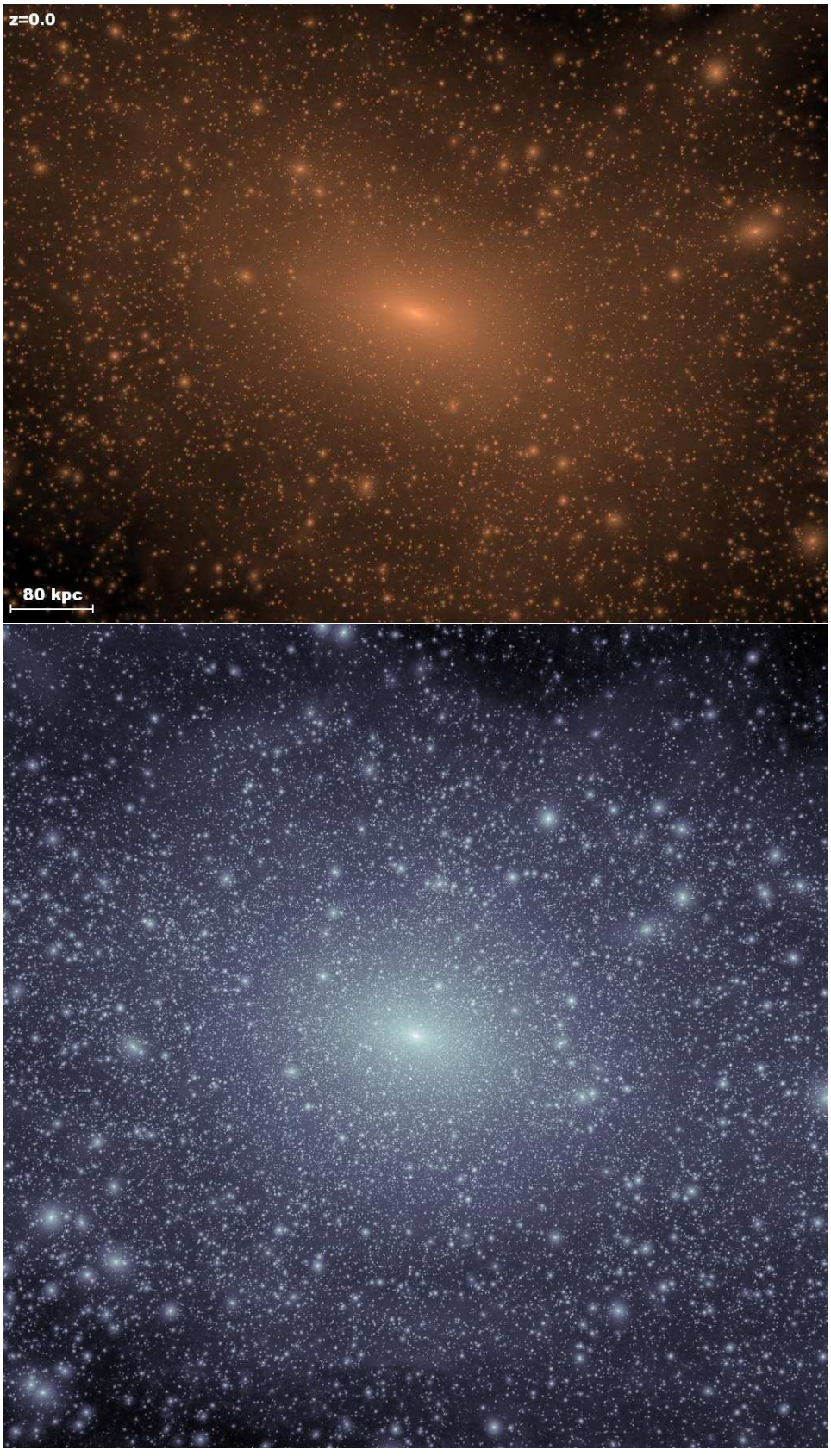

Figure 2.1: Local density maps of the dark matter halos from VL (top) and VL-2 (bottom). VL uses ~ 28 particles with a mass per particle of $21,000 M_{\odot}$. VL-2 uses five times as many particles and has a mass per particle of $4,100 M_{\odot}$. Images were taken from the Via Lactea web page [8].

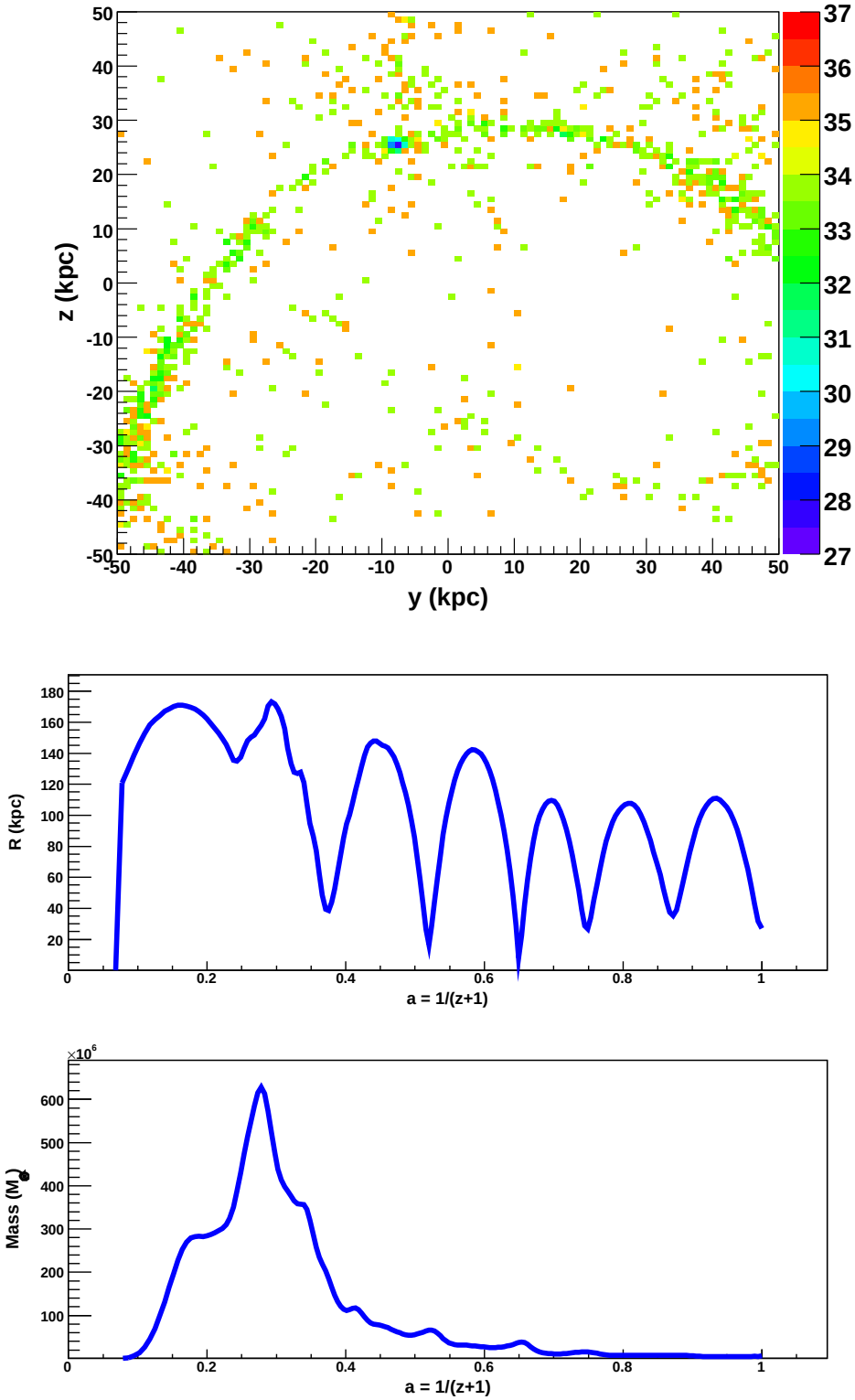

Figure 2.2: Radial and Mass evolutions with z=0 positions of an isolated subhalo. The top panel shows a surface brightness and position projection today (z=0, relative to GC) of the subhalo. It has become very elongated and spread out over one hundred kpc. Z-axis units are in $magnitudes\ arcsec^{-2}$. The bottom two panels show the evolution of the subhalo's mass and radius relative to the GC starting at z=17 to today. After the first major pass ($a \sim 0.37$) the subhalo loses over 80% of its mass, and continues to do so with each pass of the GC.

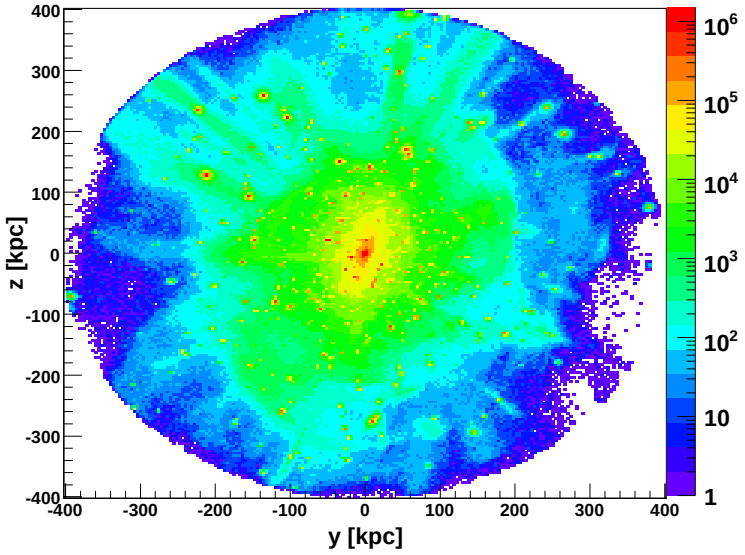

Figure 2.3: Particles within 402 kpc of the Dark Halo which formed from subhalo accretions. This plot shows a projection of the VL-2 DM halo formed by subhalos with $V_{max} > 15 kms^{-1}$ accreting onto the host halo. The Z-axis scale is the number density of particles within each pixel. This halo is the basis for the Stellar Halo when a star formation model is applied to the progenitors of the substructures.

2.1 Building the Via Lactea Stellar Halo

We implemented the prescription used by Bullock & Johnston [4] to build a stellar halo from the Via Lactea data. In this method, the history of each subhalo is used to assign gas for star formation and an efficiency of the subhalo to turn the gas into stars is considered. The cold gas mass accretion rate, $h(t)$ is set to follow the DM accretion rate, such that

$$h(t) = \frac{dM_{vir}^{sat}}{dt}[4], \tag{2.1}$$

where M_{vir}^{sat} is the virial mass of the subhalo satellite. Efficiency is taken into account by setting a fraction of cold baryonic matter to DM f_{gas}, taken by Bullock & Johnston to be 0.02. f_{gas} represents the fraction of material that is available for forming stars. The size of the subhalo is also believed to be a factor in efficiency, so another factor C, which varies like

$$C = \frac{V_{max}(kms^{-1}) - 30kms^{-1}}{20kms^{-1}} \tag{2.2}$$

is used after the time of reionization ($z_{re} = 10$). V_{max} is calculated the same way as the circular velocity, v_c, only now V_{max} is used as a general property of the subhalo's mass. Before reionization and for subhalos with $V_{max} > 50 kms^{-1}$, $C = 1$. Lastly, a time-lag for the time it takes the cold gas to settle and become dense enough for star birth is set to be $t_{in} = 6Gyr(1+z)^{-3/2}$. They assume that the star formation occurs over a time scale $t_\star$ of $15Gyr$. So now the stellar mass of a subhalo can be tracked by the following equations: [4]

$$\frac{dM_\star}{dt} = \frac{M_{gas}}{t_\star} \tag{2.3a}$$

$$\frac{dM_{gas}}{dt} = -\frac{dM_\star}{dt} + Cf_{gas}h(t - t_{in}). \tag{2.3b}$$

The stellar mass is accumulated up until the subhalo begins to accrete onto the host halo. Star formation is stopped here for simplicity, and reasoned that stellar gas could be removed via ram-pressure stripping as the subhalo falls in [4]. The time of accretion is determined by the time at which the subhalo comes within $4R_{Vmax}$, where R_{Vmax} is the proper circular speed radius of the host halo. At that point star formation is halted and the stellar mass is assigned to each particle depending on the particles distance relative to the median king core radius. The median king core radius, r_c, is the radius at which the projected density is half of the value of the core of a sphere.[2]

$$r_c = 160pc\left(\frac{L_\star(L_\odot)}{10^6 L_\odot}\right). \tag{2.4}$$

For simplicity, half of the stellar mass is distributed evenly to all particles within r_c, and the other half is distributed to all the particles within a shell $r_c < r < 2r_c$. The stellar mass is assigned as solar luminosities by assuming a stellar mass to light ratio of $M_\star/L_\odot = 2$. The luminosity is in the V, or Visual band of the spectrum [4].

2.1.1 Alterations to the Bullock Model

In both VL and VL-2, we increase the parameter f_{gas} to 0.06 to compensate for the use of different masses. Bullock & Johnston use the virial mass,

$$M_{vir} = \frac{4\pi}{3}\rho_M(z)\Delta_{vir}(z)R_{vir}^3[4], \tag{2.5}$$

where ρ_M is the average matter density of the universe and $\Delta_{vir}(z)$ is the "virial overdensity" [4]. $\Delta_{vir}(z)$ and ρ_M take on larger values in the past and so the calculated mass can be "inflated". We calculate all masses via the circular speed of the subhalo, such that

$$M_{subhalo} = \frac{V_{max}^2 R_{Vmax}}{G}, \tag{2.6}$$

where R_{Vmax} is the proper circular speed radius of the subhalo. Calculating mass in this way is more physical, in that the mass does not depend on redshift (expansionary state of the universe). It is important to note that the tracks are much more limited for VL-2 (27 as opposed to 200 snapshots for VL) so tracking mass in VL-2 requires more interpolation, perhaps resulting in a less realistic stellar halo. Because of the sparse tracks, determining the time of accretion is also more difficult for VL-2. Therefore we've taken the time of accretion for VL-2 subhalos as the time that the subhalo reaches its peak circular velocity (and therefore mass).

2.1.2 Results of Implementation

We use C++ and the "root" C/C++ interpreter to implement the Bullock method on VL and VL-2. VL has 475 contributing subhalos, resulting in a total stellar mass of $1.6 \times 10^9 M_\odot$. Six hundred and twenty five subhalos contribute to the VL-2 stellar halo totalling in $1.1 \times 10^9 M_\odot$. Both stellar halos can be seen in figures 2.5, 2.4(a) and 2.4(b).

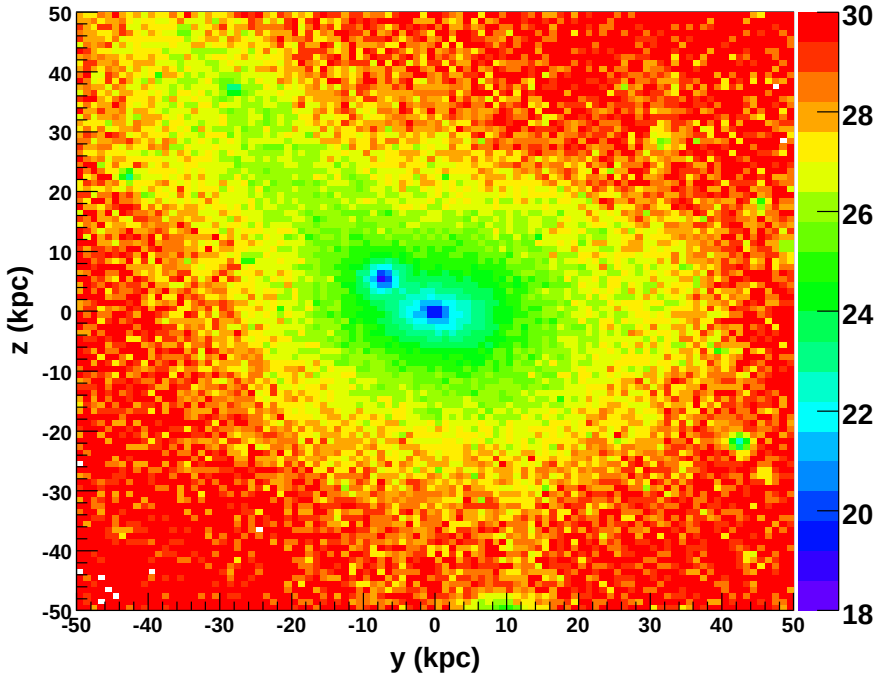

(a)

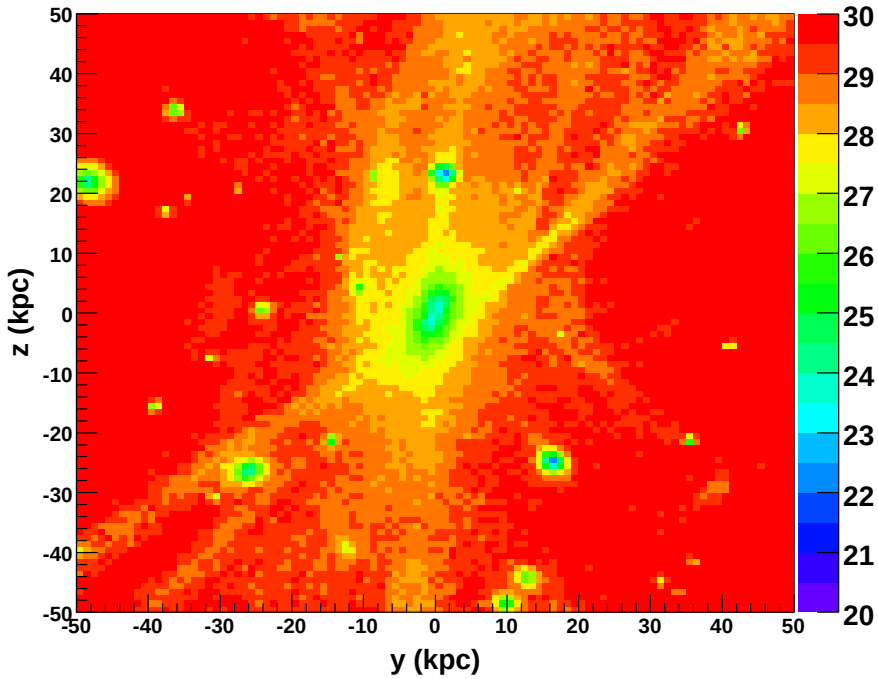

(b)

Figure 2.4: Surface brightness projection of the inner 50kpc of the VL (left) and VL-2 (right) stellar halos. Z-axis scale is in *magnitudes* $arcsec^{-2}$. For (a), the central halo appears very smooth, with a few bound objects in the outer 20kpc. For (b), the central halo has more visible structures resolved up to the very center.

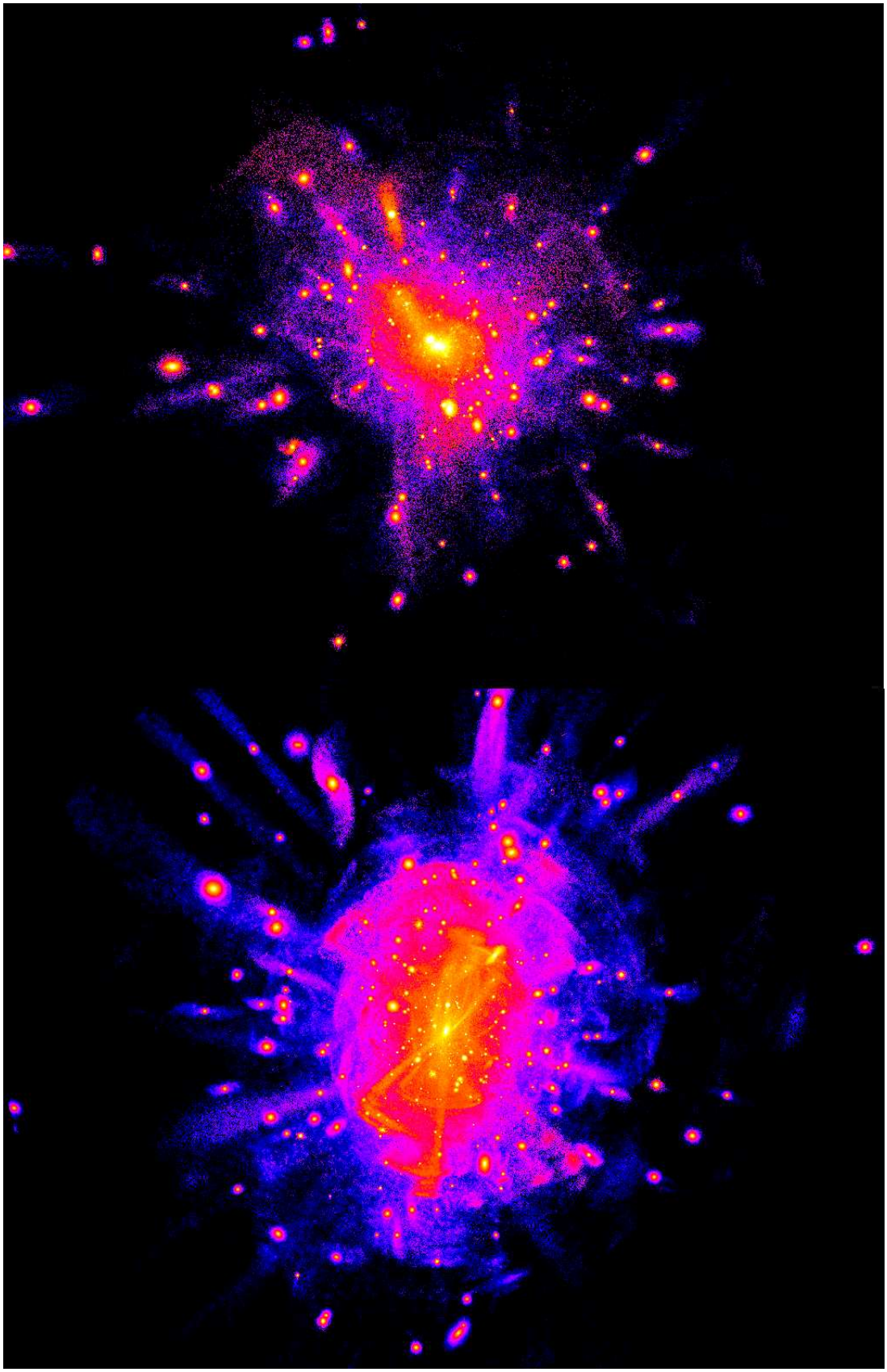

Figure 2.5: Local density projections of the stellar halos for VL (top) and VL-2 (bottom). All particles within 402kpc are shown, where the color represents the local density value ($particles\ kpc^{-3}$)for that particle on a logarithmic scale (-1 for blue and 6 for white). Densities were found with "smooth", provided by the N-body shop at the University of Washington.

3 Quantifying the Substructure

We are now in a position to provide a quantitative measurement of a stellar halo with an accretion only origin. If the Milky Way and other galaxies did indeed form from hierarchical accretions as *Via Lactea* has modeled then there should be evidence for it. The alternative (in situ formation) predicts very little substructure [1], so a resemblance to the substructure from *Via Lactea* would support an accretion origin. In quantifying substructure, we consider the efforts of others as well as the limitations of observational data. Simulation data can offer infinitely certain (as far as astronomical measurements go) information that is not readily available to observers.

3.1 Method

We take a simple approach by simulating "pencil beams" (constant solid angle lines of sight in the sky, appendix A) in VL-2. We only apply this method to VL-2 to take advantage of the higher resolution which can resolve finer substructures. The surface brightness within over lapping pencil beams of various angular sizes and radii is counted. Then the difference is found between the two beams by the following equation;

$$\sigma_r^2 = \sum_{samples} \frac{(S_{r,d\Omega_2} - S_{r,d\Omega_1})^2}{S_{r,d\Omega_2}^2}. \tag{3.1}$$

Where $d\Omega$ is the chosen angular size of the pencil beams, S is the surface brightness from all the stars in that pencil beam and within some chosen radius, and σ_r^2 is the summed value of all the variances squared from each area of the sky sampled. The surface brightness is calculated in $mag/arcsec^2$

units by

$$S(mag/arcsec^2) = M_\odot + 21.572 - 2.5log_{10}(S(L_\odot/pc^2)) \tag{3.2a}$$

$$S(L_\odot/pc^2) = 2.5log_{10}\left(\frac{A(arcsec^2)}{F(L_\odot/pc^2)}\right) \tag{3.2b}$$

Where F is the flux, $M_\odot$ is the absolute magnitude of the Sun taken to be 4.83, and A is the solid angle subtended by the object(s). Since F and A are inversely proportional to r^2, surface brightness is independent of distance. In this way, the values of σ_r^2 will not be biased towards any particular distance so only the clumpiness of substructures will be evaluated.

The argument in Eq. (3.1) will take on values $\ll 1$ if there is little variation ($S_{r,d\Omega_2} \sim S_{r,d\Omega_1}$). If there are overdensities ($S_{r,d\Omega_2} \gg S_{r,d\Omega_1}$) or underdensities ($S_{r,d\Omega 2} \ll S_{r,d\Omega_1}$) then the argument will be either $\lesssim 1$ or $\gg 1$ respectively. When the argument is summed over all areas of the sky sampled, then the value σ_r^2 will be the average value of the argument multiplied by the number of samples taken. To get an average quantity of the over all substructure σ_r^2 is normalized so that

$$\bar{\sigma}_r^2 = \sigma_r^2/N, \tag{3.3}$$

where $\bar{\sigma}_r$ is the new normalized substructure quantity and N is the number of samples. Thus values of $\bar{\sigma}_r$ that are $\lesssim 1$ or $\gg 1$ will imply an overall clumpiness at that particular radius. Values $\ll 1$ will then insinuate an overall smoothness and values in between could imply a mix.

We sample the *Via Lactea* sky with the bounds of all 360° around the azimuth, and from 30° to 60° for the elevated angles (see appendix B). A coordinate of $(\theta, \phi) = (0, 0)$ would represent the GC from our perspective. Within this area, radial distances of $\sim$ 7, 8, 11, 14, 17, 22, 28, 35kpc and a Δr of 1.0kpc are used (0.5kpc for the first radial sample, $\sim 7kpc$). All radial distances are from a perspective 8.5kpc from the GC (the Sun's position in the Milky Way). These values were chosen to correspond with current available data from the Sloan Digital Sky Survey (SDSS).

3.1.1 Meaning of $\bar{\sigma}_r$

Other groups have attempted to quantify *how much* of the Milky Way's stellar halo *is* substructure (see Bell et al. [1]). In this way, by comparing *smoothness* and *clumpiness* in a total fractional sense conclusions could be made on how much of the Milky Way stellar halo was built by accretions or in situ formation. Our method attempts to quantify the degree of *how clumpy* certain regions of the stellar halo really are. The VL-2 stellar halo is built entirely from accretions and is essentially 100% substructure, but there could still be different degrees of *smoothness* and *clumpiness*, and this is what $\bar{\sigma}_r$ is designed to do.

3.2 Analysis of the Results

The σ_r^2 values from Eq. (3.1) are plotted in the figures on the following pages. An "aitoff" projection is used just as in appendix B. In general, the smaller variations (smoother) tend to be closer to the GC (lower central area) although the GC is not directly sampled. The largest scale variations ($6 - 14°$, fig. 3.5) tend to be uniform over all the sky sampled. These variations are the smallest, and are nearly constant over the range of radii sampled (see fig. 3.1). There also appears to be little variation on the scale of $4 - 8°$ (fig. 3.4) at radii $> 7kpc$. These two scales may be too large to pick up subhalo remnants or smaller variations resulting in "smooth" quantities of σ_r.

There is a significant amount of clumpiness (more so than the $4 - 8°$ and $6 - 14°$ scales) on the scale of $2 - 4°$ (fig. 3.3) and when you look at the sky projection most of the clumpiness comes from areas away from the GC. From this, it may be that most substructure on this scale comes from remnants of accreting subhalos, which are about $4°$ in size. On the smaller scale ($1 - 2°$, fig. 3.2) there is a large amount of clumpiness, even when compared to the greatest contrasting scale of $1 - 8°$, of which it is expected that there would be large variations.

On all scales there is a consistent pattern that the stellar halo tends to become smoother as you go farther out in radius. Since the larger variations tend to occur away from the GC the

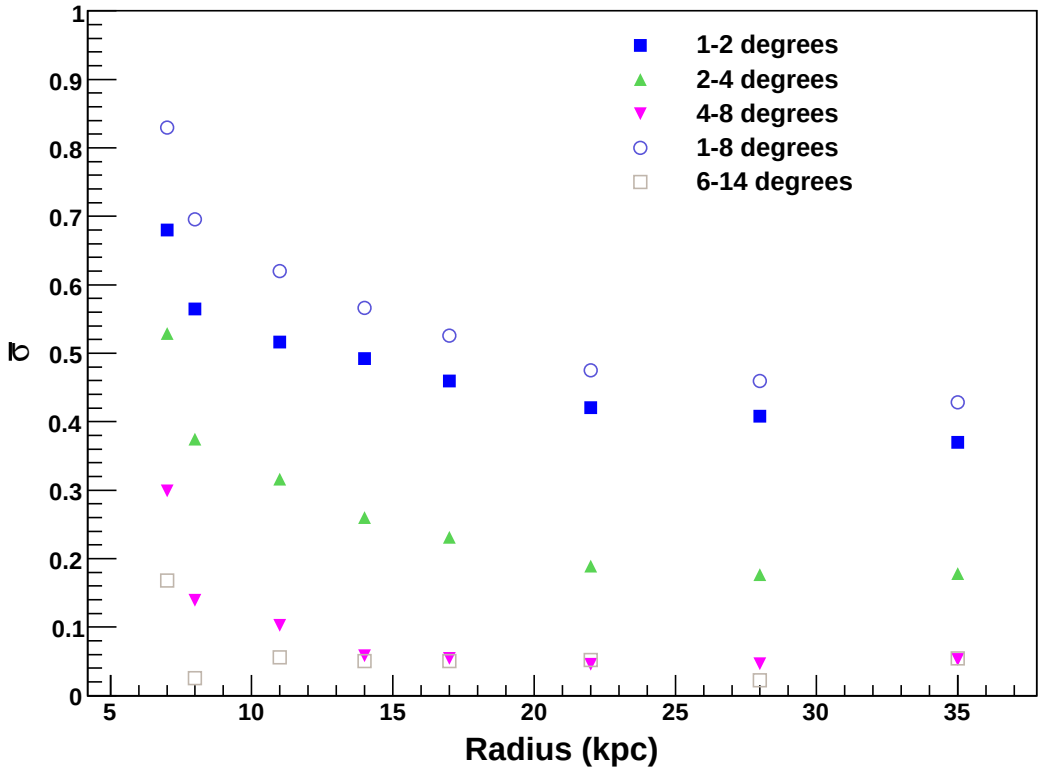

Figure 3.1: Values of $\bar{\sigma}_r$, Eq. (3.3) vs the radius, r. The scale with the most variations comes from the $1-8°$ scale. This larger scale ratio is used to aid in comparison of the other scales, since it is expected that this ratio would have the largest variations. The next most clumpy scale is $1-2°$, which is very near the $1-8°$ scale. The $4-8°$ and $6-14°$ scales are the most smooth, implying that there is little substructure on those size scales. The medium sized scale $(2-4°)$ has an intermediate range of variation.

contributions to $\bar{\sigma}_r$ could be from nearby material that is in the process of or has recently accreted onto the host halo. If so, this newly disrupted material would not have had time to settle, wiping out any variations. Material from ancient accretions dissipate fairly quickly, appearing smooth in space (Bell et al. [1]). Overall the values of $\bar{\sigma}_r$ vary from $0.2 \lesssim \bar{\sigma}_r \lesssim 0.7$ (for $1-2°$ variations) implying a mix of a smooth and clumpy stellar halo. It is difficult to determine how much of which from this method, which is a task for another project.

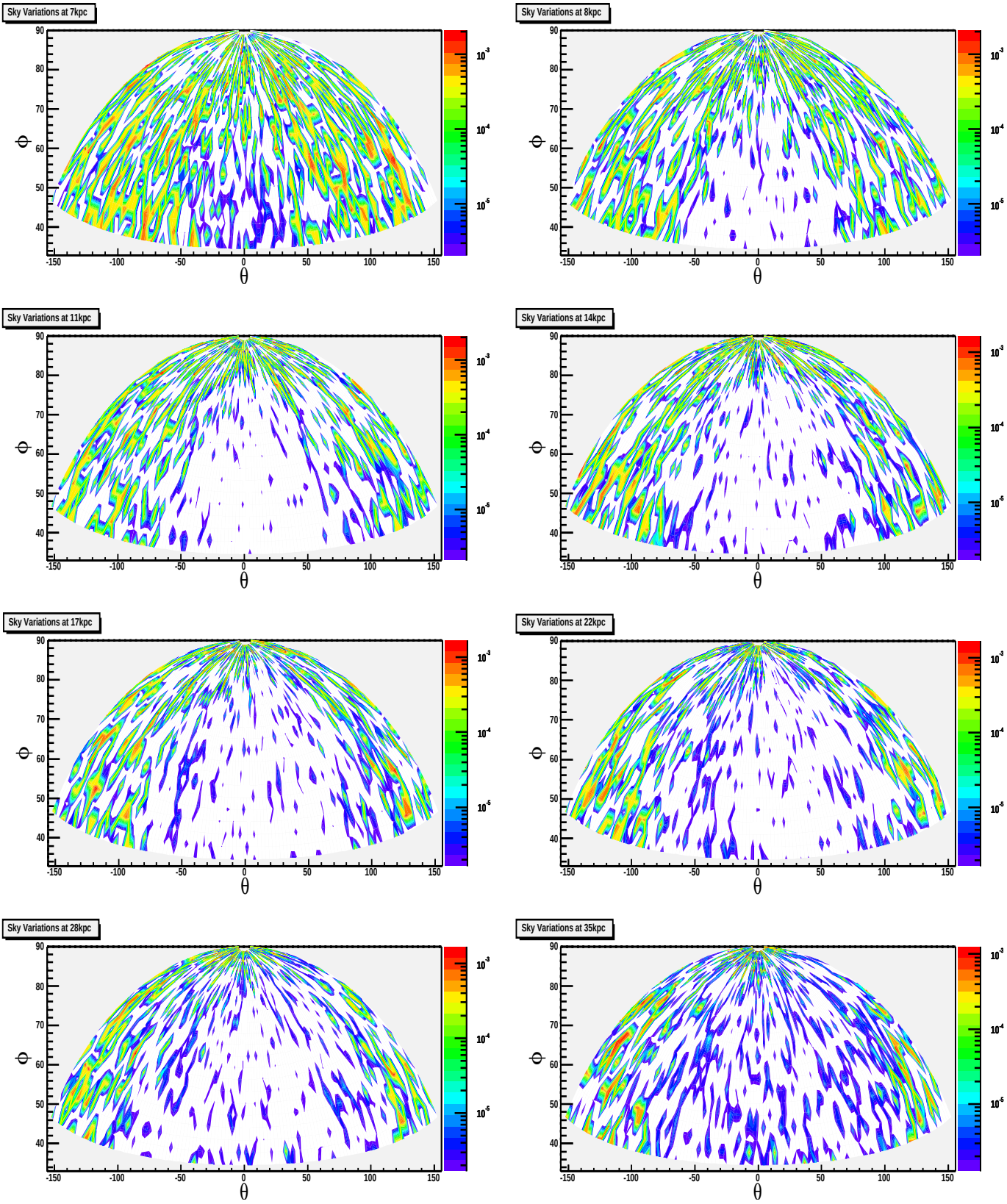

Figure 3.2: σ_r^2 values using $1-2^\circ$ pencil beams on an "aitoff" sky projection. A semi-sphere 360° around and the top 60° is used for sampling (coordinate projections are not shown, the axes only give a general idea of position). The color is on a log scale varying from 10^{-6} (purple) to 10^{-3} (red). White represents a value ~ 0.

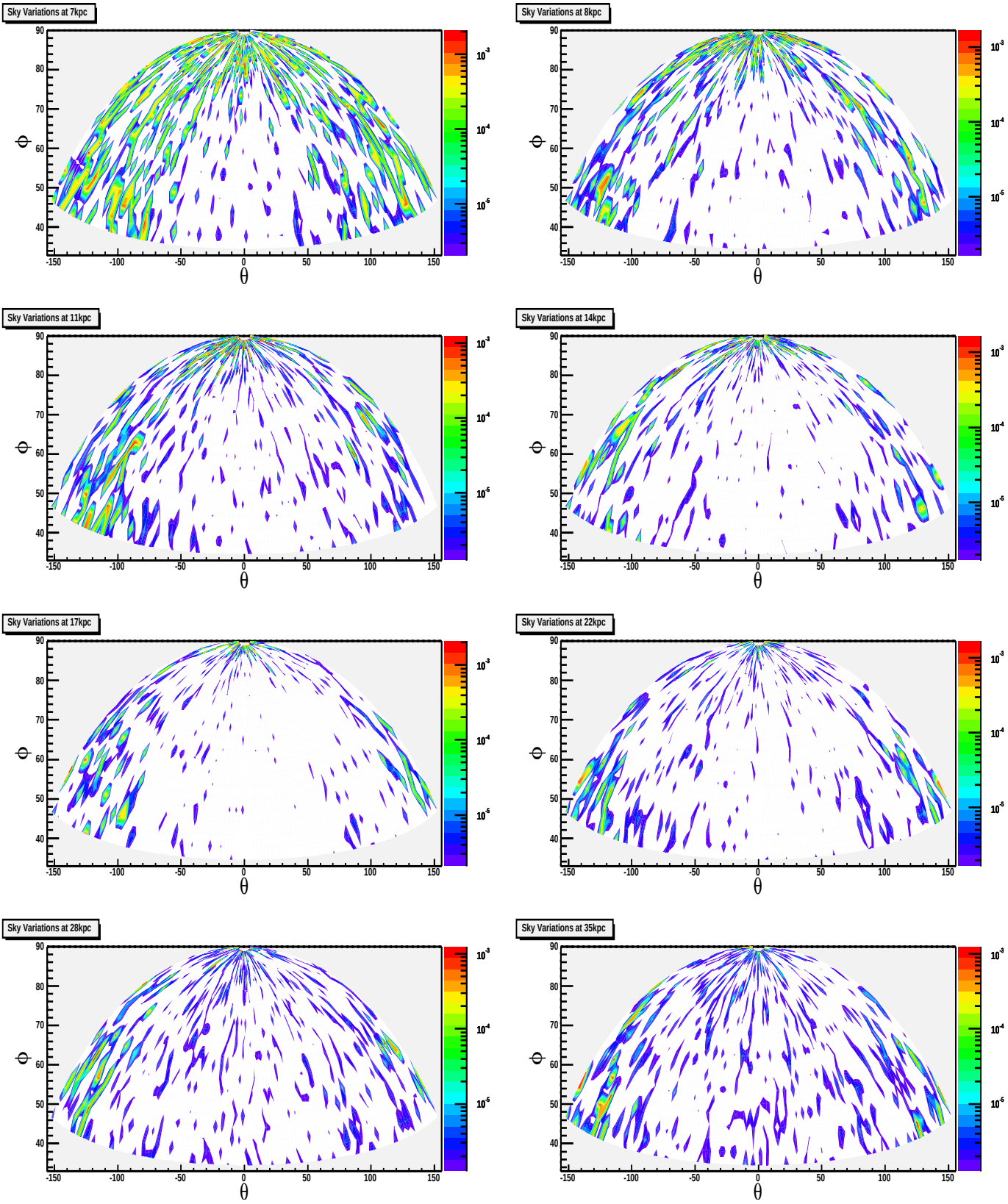

Figure 3.3: σ_r^2 values using $2-4°$ pencil beams on an "aitoff" sky projection. A semi-sphere 360° around and the top 60° is used for sampling (coordinate projections are not shown, the axes only give a general idea of position). The color is on a log scale varying from 10^{-6} (purple) to 10^{-3} (red). White represents a value ~ 0.

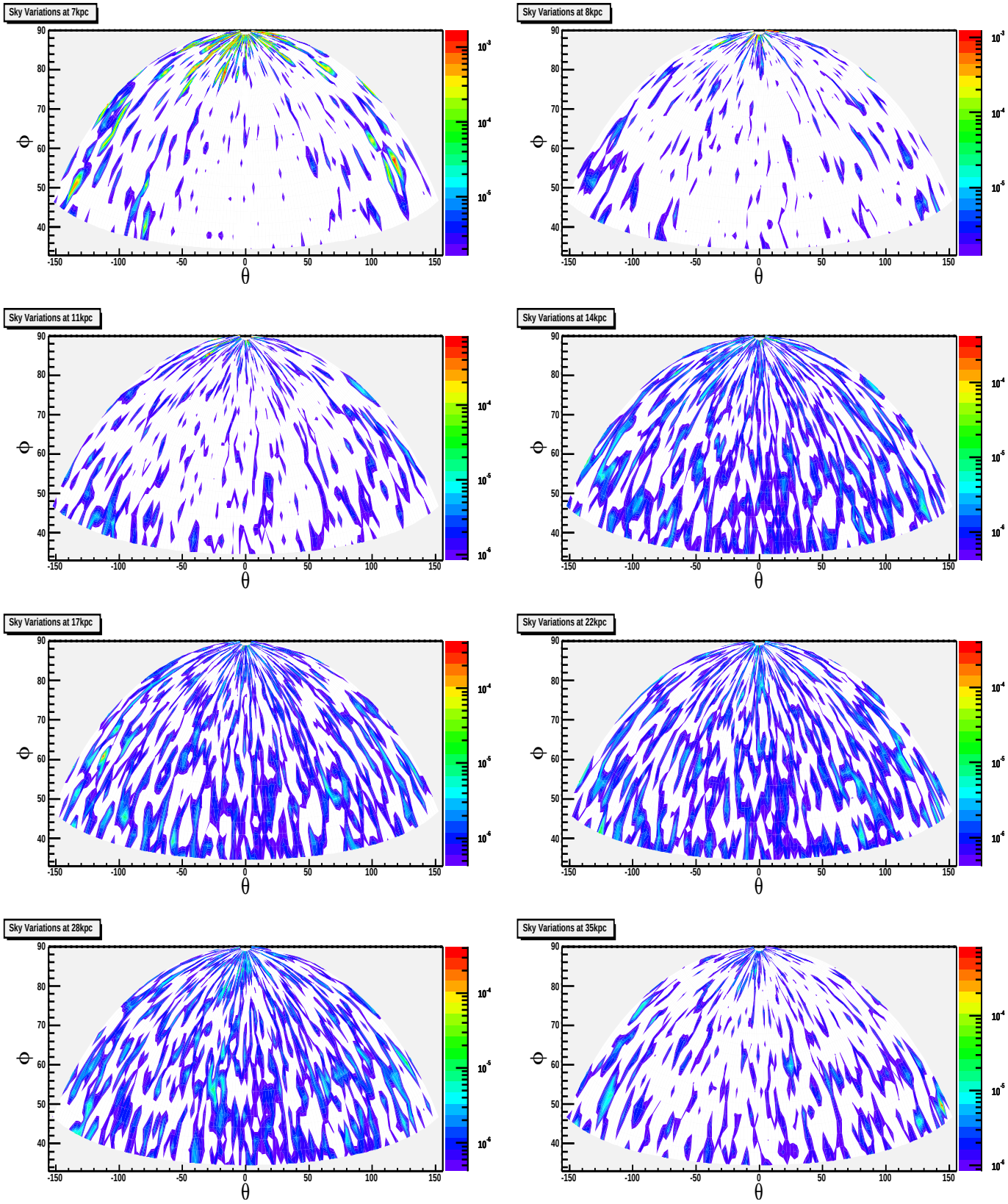

Figure 3.4: σ_r^2 values using $4-8°$ pencil beams on an "aitoff" sky projection. A semi-sphere 360° around and the top 60° is used for sampling (coordinate projections are not shown, the axes only give a general idea of position). The color is on a log scale varying from $< 10^{-6}$ (purple) to $< 10^{-3}$ (red). White represents a value ~ 0.

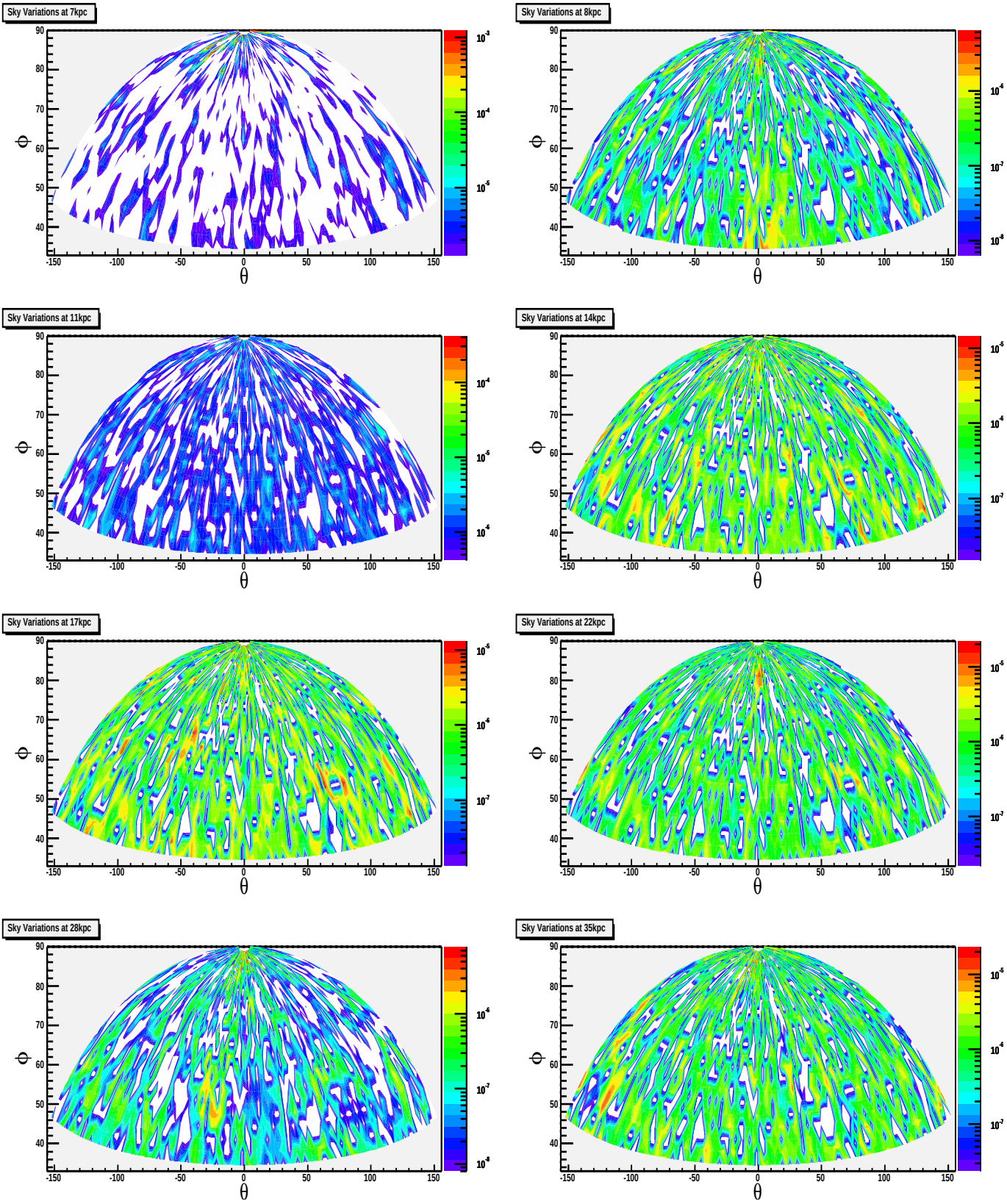

Figure 3.5: σ_r^2 values using $6-14°$ pencil beams on an "aitoff" sky projection. A semi-sphere 360° around and the top 60° is used for sampling (coordinate projections are not shown, the axes only give a general idea of position). The color is on a log scale varying from 10^{-8} (purple) to 10^{-5} (red) on the $28kpc$ panel (lower left) and reaching no more than 10^{-3} on the $7kpc$ panel (upper left). White represents a value ~ 0.

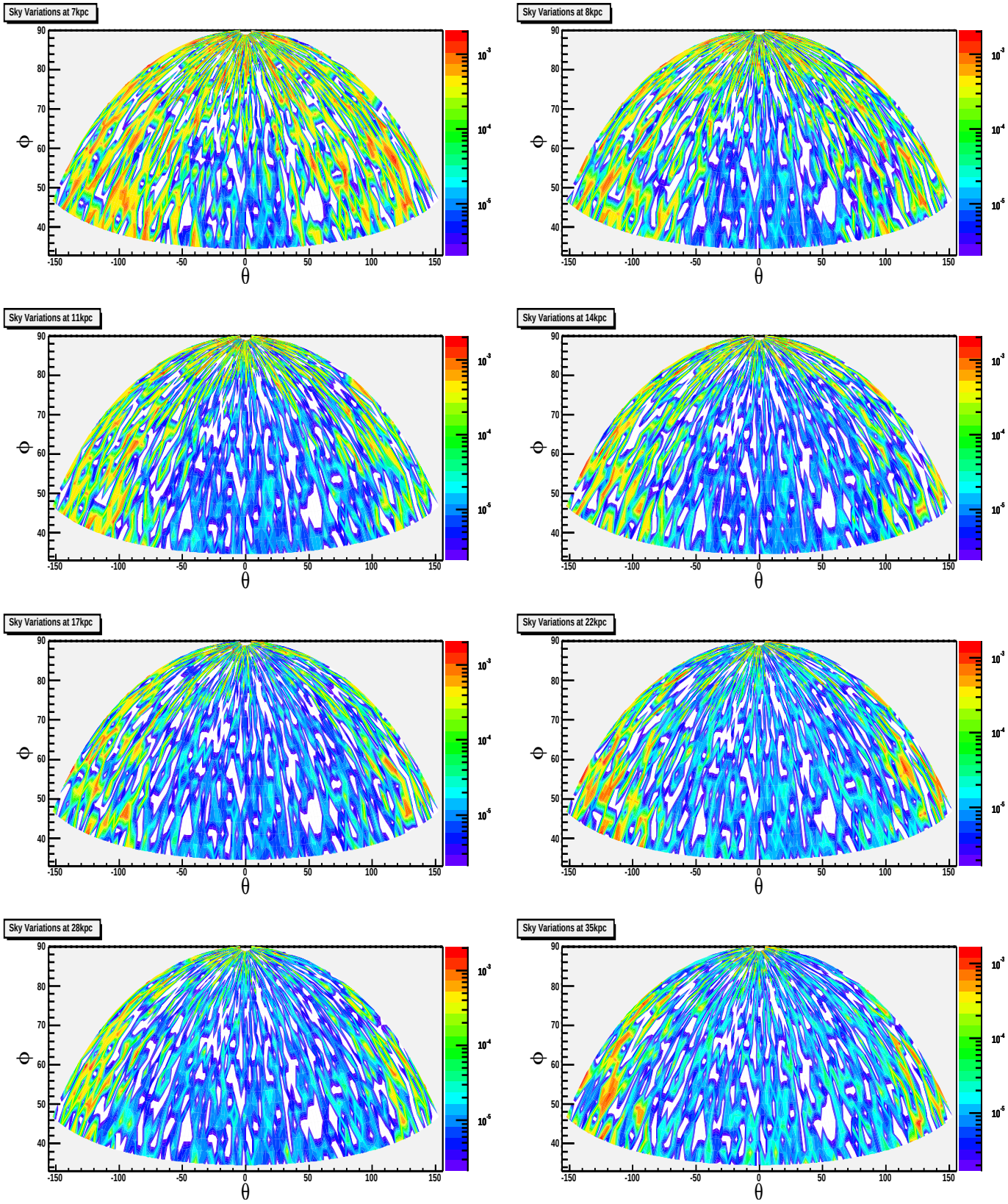

Figure 3.6: σ_r^2 values using $1-8°$ pencil beams on an "aitoff" sky projection. A semi-sphere 360° around and the top 60° is used for sampling (coordinate projections are not shown, the axes only give a general idea of position). The color is on a log scale varying from 10^{-6} (purple) to 10^{-3} (red). White represents a value ~ 0.

4 Conclusion

In this paper we have quantified the different degrees of substructure in the *Via Lactea II* stellar halo. The largest degree of variations occurred on a scale using 1° and 2° sized pencil beams, while the larger scales ($4-8°$ and $6-14°$) tended to show little variation. In general, the stellar halo exhibited values of $\bar{\sigma}_r$ inductive to a mix of clumpy and smooth structures. As the SDSS data are expanded then perhaps more detailed comparisons can be made with the latest N-body simulations.

Future prospects center around creating a more realistic model for implementing light into Cosmological N-body simulations like *Via Lactea*. Potentially, the metallicities of stars (fraction of elements higher than He) and the different populations of stars (III-I, oldest to youngest) could be tracked. It may be found that areas of the stellar halo with properties related to these may have come about from an accretion origin stellar halo. The latest simulation in the works, *Silver River* (Chinese translation for "Milky Way"), with $\sim 3 \times 10^{10}$ particles will allow further work in this field with an ever increasing resolution.

Appendix A

Pencil Beam Configuration

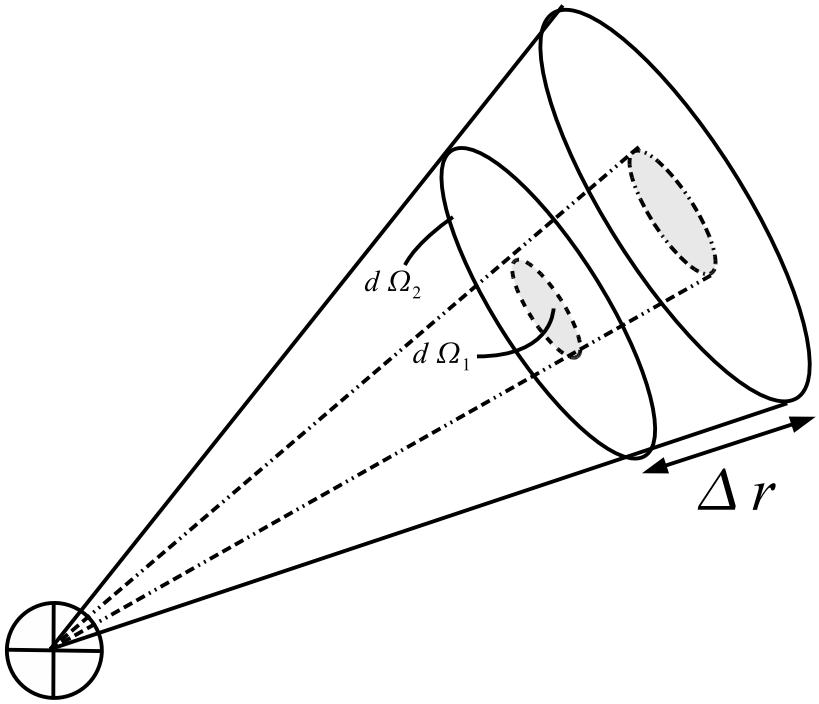

The configuration for measuring the surface brightness variations (Eq. (3.1)) in *Via Lactea*. All of the light within the volumes $d\Omega_1 \Delta r$ and $(d\Omega_2 - d\Omega_1)\Delta r$ is counted and used in calculating the surface brightness (Eq. (3.2)). The beams are a constant angular size from our perspective but at a greater radius the samples encompass more light.

Appendix B

Via Lactea Sky Sampling

The following two figures represent the VL-2 stellar halo in a "aitoff" projection. The top figure presents the total luminosity in solar luminosities per square degree squared ($L_{\odot}/degree^2$). The color scale is a log scale with purple being 1, and red being 10^3. The bottom figure is the same but only the area sampled ($30^{\circ} < \phi < 90^{\circ}$) for the quantification of the substructure is shown. This is done to coincide with available data for comparison.

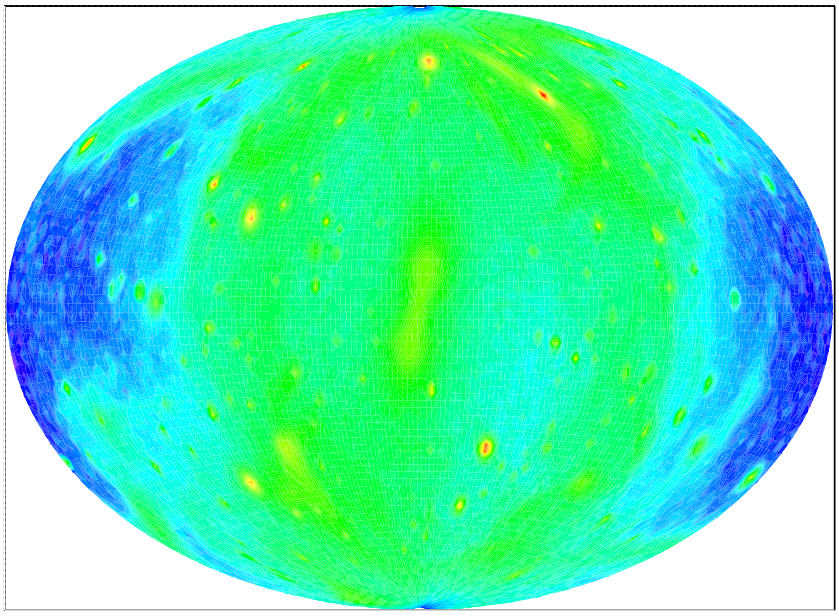

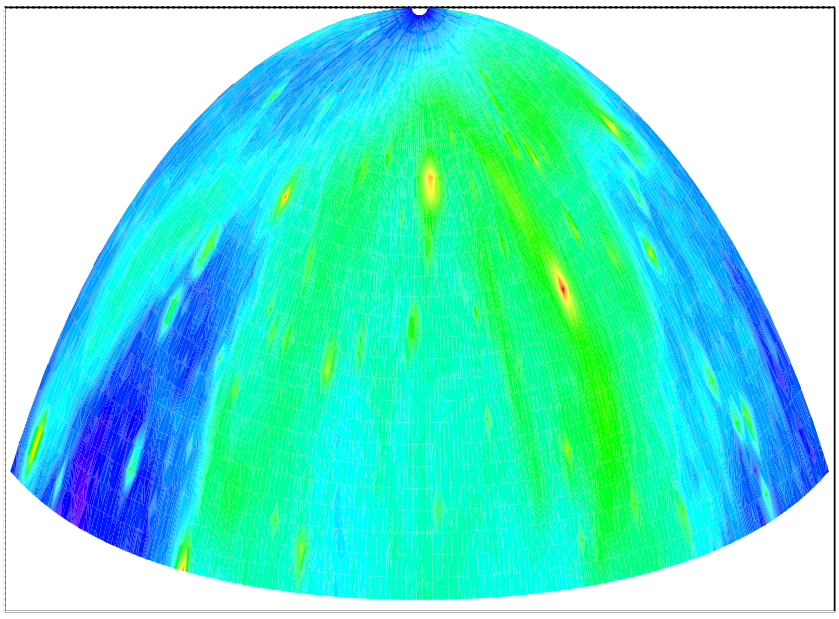

Bibliography

[1] Bell E. F., Zucker D. B., Belokurov V., et al. 2008, ApJ, 680:295-311. arXiv:0706.0004v2 [astro-ph].

[2] Binney J., Tremaine S., Galactic Dynamics. Princeton University Press, New Jersey. 1987.

[3] Britt Griswold. 7 April, 2009. http://map.gsfc.nasa.gov/

[4] Bullock J. S., Johnston K. V., 2005, ApJ, 635:931-949. ArXiv Astrophysics e-prints, arXiv:astro-ph/0506467v1.

[5] Coles, P, Lucchin, F. *Cosmology*, The Origin and Evolution of Cosmic Structure. 2nd edition. John Wiley and Sons, Ltd, West Sussex, England. 2002.

[6] Diemand, J., Kuhlen, M., Madau, P. 2007, ApJ, 667, 859, astro-ph/0703337.

[7] Diemand J., Kuhlen M., Madau P., Zemp M., Moore B., Potter D., Stadel J., 2008, Nature, 454, 735-738, astro-ph/0805.1244.

[8] Diemand J. The Via Lactea Project: High Resolution Milky Way Dark Matter Halos. 24 Nov. 2008. http://www.ucolick.org/ diemand/vl/index.html

[9] Hartle, J. B, *Gravity*, An Introduction to Einstein's General Relativity. Addison Wesley, San Francisco. 2003.

[10] G. Hinshaw, et al., 2009, ApJ, 180, 225-245. fig. 12.

[11] Ryden B., Introduction to Cosmology. Addison Wesley, San Francisco. 2003.

[12] Sarkamo, Juho. 10 April, 2003. http://cupp.oulu.fi/neutrino/nd-cross.html.

[13] PKDGRAV, Parallel K-D tree GRAVity code.
http://hpcc.astro.washington.edu/faculty/trq/brandon/pkdgrav.html.

[14] Stadel, J. G. Cosmological N-body simulations and their analysis. PhD Thesis, University of Washington (2001).